Phase stability analysis of the InAs/GaAs (001) wetting layer from first principles

John C. Thomas[*] and Joanna Mirecki Millunchick[†]

Department of Materials Science and Engineering, University of Michigan, Ann Arbor, Michigan 48109, USA

Anton Van der Ven[‡]

Department of Materials Science and Engineering, University of Michigan, Ann Arbor, Michigan 48109, USA
and Materials Department, University of California, Santa Barbara, California 93106, USA

Normand A. Modine[§]

Center for Integrated Nanotechnologies, Sandia National Laboratories, Albuquerque, New Mexico 87185, USA

The large atomic-size mismatch between In and Ga and the large lattice-mismatch strain between InAs and GaAs make the InAs/GaAs (001) growth interface a complex alloy system, the understanding of which can enhance control of device synthesis and nanostructure self-assembly. We present a detailed first-principles analysis of the full progression of surface reconstructions observed on the InAs/GaAs(001) wetting layer during early stages of In deposition. We use systematic techniques to identify the most likely surface reconstruction prototypes of the InAs wetting layer on GaAs(001) using density functional theory (DFT) and then develop several cluster expansion Hamiltonians in order to thoroughly explore surface alloy disorder due to species substitution of In, Ga, and As at the surface. We use these results to construct a first principles 0-K surface phase diagram of the InAs wetting layer on GaAs(001) and test the sensitivity of our predicted phase diagram to DFT approximations and convergence errors. We find two alloy configurations of the (4×3) structural prototype that are likely ground-state surface reconstructions, and simulated scanning tunneling micrographs (STM) of these reconstructions indicate that they can explain prominent features of experimentally obtained STM of the InAs/GaAs (4×3) surface.

PACS number(s): 68.35.Md, 68.35.B−, 68.47.Fg

I. INTRODUCTION

The richness of atomic structure and ordering phenomena at the surface of semiconductor alloys generally, and III-V alloys in particular, presents potential engineering pathways for optimizing and controlling material behavior and device performance. The strong interplay between atomic surface structure and surface alloy ordering, which together specify the surface *reconstruction*, can significantly influence bulk alloy ordering due to 2D correlation at the growth surface becoming kinetically trapped within the growing crystal [1]. Atomic surface structure on size-mismatched alloys has also been implicated in surface segregation enhancement, which can lead to improved interface abruptness at semiconductor heterojunctions [2] and consequent measurable improvements in *I*-*V* characteristics of the resulting device [3].

Unfortunately, the complexity of surface structure and ordering phenomena, in addition to providing exciting opportunities for enhancing synthesis capabilities, also presents a significant challenge to the characterization and prediction of atomistic details of compound semiconductor surfaces, even at equilibrium. The under-coordination of atoms at the surface gives rise to a preponderance of low-energy degrees of freedom related to both the structural rebonding of surface atoms and

the configurational exchange of species at atomic surface sites, which can only be described within a high-dimensional parameter space. First-principles electronic structure methods such as density functional theory (DFT) are now widely employed to calculate and compare the energies of hypothesized surface structures and alloy configurations in order to identify the ground-state surface reconstructions that occur at equilibrium. However, the low-energy parameter space is simply too vast to explore exhaustively via a combinatorial approach using DFT alone; for GaAs and its alloys, an impractically large number of (001) surface reconstructions are known to lie within no more than 25 meV/$A_{(1\times1)}$ of the surface reconstruction ground states, where $A_{(1\times1)}$ is the area of a (1×1) surface unit cell [4–6].

Recent work has demonstrated the feasibility of systematizing the search for ground-state surface reconstructions into a two-step process [4]. The first step consists of a structural search for likely surface reconstructions prototypes. The second step is a search for symmetrically distinct ways of decorating the reconstruction prototype with different alloying elements. The structural search consists of an automated enumeration of surface reconstruction bonding topologies, based upon known low-energy structural motifs; the resulting database of enumerated bond topologies, or reconstruction *prototypes*, can subsequently be screened for fitness using a combination of heuristic and first-principles tests. Once energetically favorable prototype reconstructions have been found, low-energy ordering of alloying elements over the sites of the prototype are enumerated with the help of a cluster expansion Hamiltonian [7], parameterized by fitting to a database of surface energies calculated from first

—————
[*]johnct@umich.edu
[†]joannamm@umich.edu
[‡]avdv@engineering.ucsb.edu
[§]namodin@sandia.gov

principles for a small subset of different alloy compositions and orderings.

Due to the low surface energy of InAs and large In–As bond length, relative to GaAs, InAs exhibits surfactant behavior at the GaAs(001) surface. Despite the immiscibility of bulk InAs and GaAs, InAs deposited on GaAs wets the surface to form a two-dimensional alloy [8] that tends to segregate as a floating layer if additional GaAs is subsequently deposited [9]. At a critical InAs wetting layer thickness in the range of 1.2–1.5 ML, depending on temperature, the surface morphology undergoes a transition from two-dimensional to three-dimensional islands [10]. When properly encapsulated within a thin-film heterostructure, these self-assembled islands behave as quantum dots [11], whose tunable electronic properties can be harnessed for device applications. Experiments indicate that the surface undergoes a characteristic sequence of reconstruction transitions during this process [12,13]. Starting from the $c(4 \times 4)$ surface of GaAs(001), deposition of InAs induces a transition first to a $(n \times 3)/(4 \times 3)$ phase and then to a (2×4) phase before three-dimensional islands begin to form in the vicinity of 1.4 ML InAs. Quantum dots can also form via an As-induced conversion reaction of In nanocrystals into InAs, in which case the reconstruction present prior to In deposition seems to significantly impact the resulting film morphology and dot uniformity [14].

Our previous work on the InAs/GaAs (001) wetting layer, which considered only the $\alpha2(2 \times 4)$ and $\beta2(2 \times 4)$ surface structures as model examples, elucidated the strong influence that alloying can have on the order and phase stability of the surface reconstruction [15]. By constructing a model that coupled alloy degrees of freedom to structural degrees of freedom, we were able to suggest basic guidelines to anticipate the ways in which alloying the surface with a size-mismatched species may affect its atomic structure. However, the limited nature of the model used to obtain those results made it unsuitable for making detailed or specific predictions concerning surface reconstruction phase stability, as such an analysis would have required a comparison of the (2×4) reconstruction phase to other potentially stable reconstructions.

In this paper, we use density functional theory, along with the cluster expansion formalism [7,16], to better understand the full progression of surface reconstructions that is observed on the InAs/GaAs(001) wetting layer during early stages of In deposition. To this end, we consider the effects of atomic-size mismatch strain on the structural and configurational phase stability over the entire range of anion-rich surface reconstructions of GaAs(001) in order to reveal the alloying response of the system. Using these results, we construct a first-principles 0-K surface phase diagram of the InAs/GaAs(001) wetting layer. We also perform a sensitivity analysis of our predicted phase diagram in order to determine the effect of approximations or convergence errors on our results. The phase diagram reveals two predominant alloy configurations of the (4×3) structural prototype that are likely to be reconstruction ground-states, and simulated scanning tunneling micrographs (STM) of these reconstructions suggest that they explain prominent features of experimentally-obtained STM of the InAs/GaAs (4×3) surface.

A. Reconstructions of the InAs/GaAs(001) wetting layer

Experimental evidence indicates that the alloying degrees of freedom created when In is deposited onto the GaAs(001) surface significantly extend the range of thermodynamically accessible surface reconstructions. On pure GaAs(001), as has been described in detail previously [4,5,17–21], the surface can generally be described as passing through a number of distinct surface phases—from $\zeta(4 \times 2)$ to $\beta2(2 \times 4)$ to $\beta(4 \times 3)$ to $c(4 \times 4)$-α and, finally, to $c(4 \times 4)$-β—as the surface is taken from Ga-rich to As-rich conditions. Observations of the InAs wetting layer, however, indicate that it departs from this progression in a number of ways. Starting from the GaAs-(2×4) surface under relatively low As overpressure, alloying with In tends to disorder the surface while maintaining its (2×4) periodicity [12,13], and both $\beta2(2 \times 4)$ and $\alpha2(2 \times 4)$ can be observed with STM on the resulting surface [22]. Under As-rich conditions, where the starting surface is GaAs-$c(4 \times 4)$, In deposition induces a transition to a poorly-ordered $(n \times 3)$ surface, according to RHEED measurements [12]. High-resolution STM of this alloyed $(n \times 3)$ phase on the InAs/GaAs wetting layer indicates that, at least under some conditions, it is comprised of (4×3) unit cells that are misaligned along the $[1\bar{1}0]$ direction [13,22]. In this sense, it is similar to the $(n \times 3)$ phase on the Bi/GaAs(001) wetting layer, which comparisons of measured and simulated STM have shown to also likely be comprised of a (4×3) unit cell [23].

Although few theoretical findings exist for the structure of the 2D InAs/GaAs wetting layer, previous theoretical investigation of alloying on the InAs/GaAs surface at the $In_{0.5}Ga_{0.5}As$ lattice parameter did predict alloy-driven stabilization of the $\alpha2(2 \times 4)$ reconstruction at 0 K [24]. Calculations also show that, relative to $\beta2(2 \times 4)$ and $\zeta(4 \times 2)$, the $\alpha2(2 \times 4)$ can be stabilized by isotropic compressive strain on GaAs(001) [25]. This prediction, when considered alongside the large atomic size mismatch between In and Ga (InAs has a lattice parameter 7% larger than that of GaAs), suggests that the observation of $\alpha2(2 \times 4)$ on the alloyed surface may be due to an effective surface stress induced by surface enrichment of In, which is size-mismatched relative to the bulk substrate, which remains at the GaAs lattice parameter [26]. Few theoretical studies of $(n \times 3)$ reconstructions have been performed for GaAs-based surface systems. However, the stability of various $(n \times 3)$ reconstructions has been tested on $In_{0.5}Ga_{0.5}As$ (001) using density functional theory, and the only $(n \times 3)$ reconstruction predicted to be stable is restricted to a small region of chemical potential at extremely As-rich conditions [24]. It is described by a (2×3) unit cell that, according to the electron counting rule, is not charge-balanced.

II. METHODOLOGY

Our strategy to predict the reconstruction phase stability of the InAs/GaAs(001) wetting layer is based on a systematic approach conducted in two steps. First, we select the set of most likely surface reconstruction prototypes for the system, as determined from extensive enumeration and first-principles electronic structure calculations. Second, for each of the most likely prototypes, we explore the dependence of its surface energy on the configuration of atomic species (i.e., In, Ga, and As)
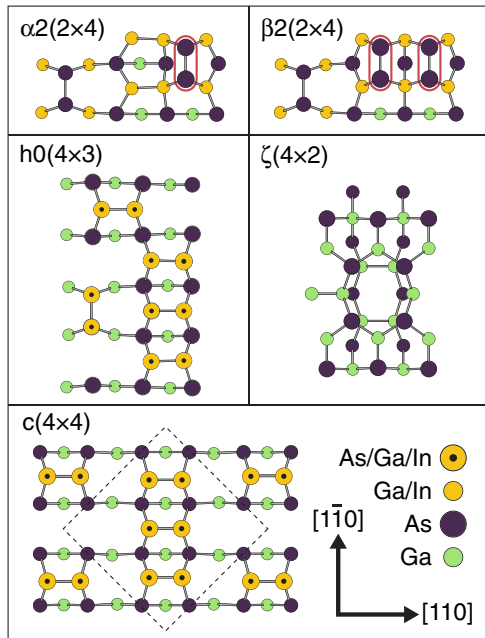
FIG. 1. (Color online) Illustration of the surface reconstruction prototypes considered for constructing the InAs/GaAs(001) surface phase diagram. Green (Ga) and purple (As) circles indicate sites whose species is fixed in all configurations. Gold circles indicate sites that can undergo Ga/In substitution, and gold circles with black centers indicate sites that can undergo As/Ga/In substitution. Circled dimers in the (2×4) prototypes indicate that these As dimers can undergo chemisorption/desorption.

over the subset of its surface sites that can accommodate low-energy species substitution. The first step of this process was presented in previous work [4], in which we reported in detail on the prototypes most likely to occur on the pure GaAs(001) surface and confirmed the well-accepted models for the GaAs-(2×4) [dubbed $\beta2(2 \times 4)$] and GaAs-$c(4 \times 4)$. We additionally identified the most likely model for the GaAs-(4×3), which is experimentally observed at low temperature. These prototypes are all shown in Fig. 1, in addition to the $\alpha2(2 \times 4)$, which is a variant of the $\beta2(2 \times 4)$ that is nearly stable on GaAs(001). Figure 1 also includes the $\zeta(2 \times 4)$, which exhibits planar sp^2-type bonding, a structural motif not considered in our original enumeration algorithm. It is observed on GaAs(001) under very Ga-rich conditions [27].

For each of the prototypes illustrated in Fig. 1, we specify the accessible alloying degrees of freedom by identifying sites of the prototype at which there is a low substitution energy of In for Ga or, in some cases, of a cation (i.e., In or Ga) for As. In-Ga substitution is an isovalent process that occurs readily at the surface but becomes less energetically favorable at subsurface sites due to the large mismatch in optimal lengths for In–As bonds relative to Ga–As bonds [28]. As-cation substitution is most energetically favorable at an As–As surface dimer, forming a III-V heterodimer. As suggested by the electron counting heuristic [29] and verified by DFT calculations, it is generally possible for surface sites with threefold coordination (which include the sites of surface dimers) to undergo nonisovalent substitution while maintaining perfect filling of the valence-band surface electronic

states. However, nonisovalent surface substitution is typically accompanied by large local relaxations, as the three-fold-coordinated cation attempts to acquire an sp^2-type bonding environment, while the three-fold-coordinated anion attempts to acquire an sp^3-type bonding environment [30]. In this study we have limited As-cation substitution to the dimer sites of the (4×3) and $c(4 \times 4)$. Initial energy calculations of As-cation substitution on the GaAs-(2×4) prototypes showed a very large substitution energy, likely due to the consequent formation of cation-cation bonds, which are unfavorable under As-rich conditions. As such, As-cation substitution on the (2×4) was not considered. The sites that can undergo nonisovalent substitution are denoted in Fig. 1.

Due to the large bonding radius of In relative to Ga and the strong surfactant effect of InAs on GaAs(001), there is a strong thermodynamic driving for In to segregate to the surface. Although In could isovalently substitute for Ga at any bulk cation site, the substitution energy increases significantly for sites below the surface [28]. As such, we only consider In-Ga substitution in the first subsurface layer. Since only the (2×4) prototypes possess cation sites in their first subsurface layer, they are the only ones for which isovalent substitution is considered. For the (2×4) prototypes, we also consider As-dimer chemisorption/desorption (i.e., varying the configuration of As dimers and dimer vacancies), thus allowing both the $\alpha2(2 \times 4)$ and $\beta2(2 \times 4)$ variants to be described on the same lattice model. This is the same combined substitution/adsorption model used previously to study (2×4) alloying [15].

We do not consider alloying in the $\zeta(4 \times 2)$ and thus treat it instead as a Ga-rich reference state. Although $\zeta(4 \times 2)$ may be able to accommodate some degree of In substitution, evidence suggests that alloying should not enhance its stability. The $\zeta(4 \times 2)$ is predicted to become less stable, relative to the $\alpha2(2 \times 4)$ under compressive strain on GaAs(001) [25], and experimental characterization of the (4×2) surface of InAs(001) suggests that when the surface becomes In rich it is likely described by an altogether different reconstruction prototype [31]. Nevertheless, at least one first-principles alloying study of ζ-type reconstructions has been performed, although its stability was only considered relative to a limited set of other cation-rich (4×2) reconstructions [32].

The alloying degrees of freedom were explored by calculating DFT surface energies for a number of In/As/Ga configurations of each reconstruction prototype. All DFT calculations were performed in the self-consistent Kohn-Sham framework as implemented in the Vienna *ab-initio* simulation package (VASP) [33]. Calculations were performed using the local density approximation (LDA) to the exchange-correlation functional [34], as parameterized by Perdew and Zunger [35]. The calculations utilize ultrasoft pseudopotentials [36] to describe the effective potential on valence-shell electrons due to each ion and its core-shell electrons. Under these conditions, the DFT energy for GaAs is converged using a plane-wave energy cutoff of 203 eV. In order to reproduce the geometry of a physical crystal interface, we performed calculations using a slab of bulklike material sufficiently thick so as to approximate the continuation of bulk below the surface. The slab is terminated above the top layer by the reconstructed

surface, and its bottom atomic bilayer is fixed at the bulk GaAs lattice parameter, as determined by LDA DFT ionic relaxation of the bulk. Atoms in all other layers, and in the reconstructed surface, are allowed to relax to the local energy minimum. The slab is separated from its periodic image by approximately 12 Å of vacuum, and its bottom surface is passivated by a layer of pseudohydrogen, with nuclear charge $Z = 0.75$, to passivate the dangling bonds of the bottom cleaved surface, in accordance with the electron counting rule [29]. Given the large size of the calculation geometry, the use of LDA allows a favorable compromise between accuracy and computational cost, especially considering that comparisons of LDA to the generalized gradient approximation have not demonstrated that one performs appreciably better than the other in predicting bulk properties of GaAs [37].

DFT calculations for the reconstructed surface typically range in size from 90–280 atoms, which is relatively large for a DFT calculation. We can nevertheless obtain good convergence of relative energies, to within a few meV, with respect to the size of the Γ-centered k-point grid by using a k-point density of at least 144 k points per reciprocal primitive cell. We only use a single k point in the reciprocal direction perpendicular to the surface, as the electron energy bands are very flat in this direction due to the vacuum separation.

Surface reconstruction stability is determined by finding the surface reconstruction that minimizes the surface free energy, γ, for a particular set of thermodynamic parameters. The surface free energy is determined by comparing the energy of the reconstructed slab to the energy of a thermodynamically comparable amount of bulklike substrate material. It is convenient, however, to first express the energy of the slab relative to several 0-K fixed-energy bulk reference states as the slab formation energy:

$$E_f^{(\text{slab})} = E_{\text{DFT}}^{(\text{slab})} - N_{\text{As}}^{(\text{slab})}\mathcal{E}_0^{(\text{As})} - N_{\text{Ga}}^{(\text{slab})}\left(\mathcal{E}_0^{(\text{GaAs})} - \mathcal{E}_0^{(\text{As})}\right)$$
$$- N_{\text{In}}^{(\text{slab})}\left(\mathcal{E}_0^{(\text{InAs})} - \mathcal{E}_0^{(\text{As})}\right) - N_{(1\times1)}E_f^{(\text{pass})}, \quad (1)$$

where $\mathcal{E}_0^{(\text{As})}$ is the DFT energy per atom of bulk As in its $A7$ phase, $\mathcal{E}_0^{(\text{InAs})}$ is the DFT energy per formula unit of zinc-blende InAs, and $\mathcal{E}_0^{(\text{GaAs})}$ is the DFT energy per formula unit of zinc-blende GaAs. Together, these bulk phases specify reference energies for As, In, and Ga, respectively [38]. $E_{\text{DFT}}^{(\text{slab})}$ is the DFT energy of a surface slab terminated by the reconstruction under consideration. $N_i^{(\text{slab})}$ is the number of atoms of each species i contained in the slab, and $N_{(1\times1)}$ is the number of (1×1) surface cells contained in the slab calculation geometry. $E_f^{(\text{pass})}$ is the formation energy of the bottom pseudohydrogen passivation layer, per (1×1) surface cell, determined by comparing the energies of two GaAs slabs of different thicknesses, each passivated on both sides with pseudohydrogen. The passivation correction $E_f^{(\text{pass})}$ also includes contributions from a half-monolayer of As, which is necessary due to the calculation geometry.

The surface free energy is found by expressing the first and second laws of thermodynamics for the surface formation and enforcing equilibrium of the surface with the bulk substrate. The first and second laws yield the change in formation energy

of the slab:

$$\mathrm{d}E_f^{(\text{slab})} = T\,\mathrm{d}S^{(\text{slab})} + \mu_{\text{As}}\,\mathrm{d}\widetilde{N}_{\text{As}}^{(\text{slab})} + \mu_{\text{Ga}}\,\mathrm{d}N_{\text{Ga}}^{(\text{slab})}$$
$$+ \mu_{\text{In}}\,\mathrm{d}N_{\text{In}}^{(\text{slab})} - P\mathrm{d}V^{(\text{slab})} + \gamma A_{(1\times1)}\,\mathrm{d}N_{(1\times1)}, \quad (2)$$

where μ_i are the chemical potentials of each species i, and $\widetilde{N}_{\text{As}}^{(\text{slab})} \equiv (N_{\text{As}}^{(\text{slab})} - N_{(1\times1)}/2)$ reflects the As contribution to the passivation layer correction in Eq. (1). Because we are working in terms of the slab formation energy, all chemical potentials are defined relative to the fixed-energy bulk reference states. $A_{(1\times1)}$ is the area of a (1×1) surface unit cell in a particular Lagrangian reference state, and because elastic effects are not considered, the in-plane lattice parameter is always fixed to that of the bulk substrate. The DFT calculations are performed in the limit of $P \to 0$ and $T \to 0$, so that temperature and pressure terms can be neglected.

It is convenient to perform the change of variables

$$N_{\text{Ga}}^{(\text{slab})} \equiv N_{\text{cat}}^{(\text{slab})} - N_{\text{In}}^{(\text{slab})}, \quad (3)$$

where $N_{\text{cat}}^{(\text{slab})}$ is the number of cations in the slab. We find that this casts the problem in the context of alloy substitution of cation species, with Eq. (2) becoming, after substituting Eq. (3) and taking the limits $P \to 0$ and $T \to 0$,

$$\mathrm{d}E_f^{(\text{slab})} = \mu_{\text{As}}\,\mathrm{d}\widetilde{N}_{\text{As}}^{(\text{slab})} + \mu_{\text{Ga}}\,\mathrm{d}N_{\text{cat}}^{(\text{slab})}$$
$$+ \Delta\mu_{\text{cat}}\,\mathrm{d}N_{\text{In}}^{(\text{slab})} + \gamma A_{(1\times1)}\,\mathrm{d}N_{(1\times1)}, \quad (4)$$

where $\Delta\mu_{\text{cat}} \equiv \mu_{\text{In}} - \mu_{\text{Ga}}$ is the relative cation chemical potential. Equation (4) describes a homogeneous equation of degree 1 with respect to scaling the amount of slab under consideration. Application of Euler's theorem for homogenous functions thus yields the integral equation:

$$E_f^{(\text{slab})} = \mu_{\text{As}}\widetilde{N}_{\text{As}}^{(\text{slab})} + \mu_{\text{Ga}}N_{\text{cat}}^{(\text{slab})}$$
$$+ \Delta\mu_{\text{cat}}N_{\text{In}}^{(\text{slab})} + \gamma A_{(1\times1)}N_{(1\times1)}, \quad (5)$$

where temperature and pressure terms have been neglected, and all quantities specified by $X^{(\text{slab})}$ are determined by the calculation geometry.

Solving Eq. (5) for the surface free energy γ, we find

$$\gamma = \left[E_f^{(\text{slab})} - \mu_{\text{As}}\widetilde{N}_{\text{As}}^{(\text{slab})} - \mu_{\text{Ga}}N_{\text{cat}}^{(\text{slab})}\right.$$
$$\left. - \Delta\mu_{\text{cat}}N_{\text{In}}^{(\text{slab})}\right]/(A_{(1\times1)}N_{(1\times1)}). \quad (6)$$

From a practical standpoint, Eq. (6) is still ill-defined, since the thickness of the surface slab (which determines the various $N_i^{(\text{slab})}$) is arbitrary. An additional constraint must be imposed, which is that the surface is at equilibrium with the bulk crystalline substrate. The formation energy for a formula unit of bulk $\text{In}_y\text{Ga}_{1-y}\text{As}$, obtained similarly to Eq. (5), is

$$E_f^{(\text{In}_y\text{Ga}_{1-y}\text{As})} = E_{\text{DFT}}^{(\text{In}_y\text{Ga}_{1-y}\text{As})} - y\mathcal{E}_0^{(\text{InAs})} - (1-y)\mathcal{E}_0^{(\text{GaAs})}$$
$$= \mu_{\text{As}} + \mu_{\text{Ga}} + y\Delta\mu_{\text{cat}}. \quad (7)$$

Because the surface is in equilibrium with the substrate, the chemical potentials appearing in Eq. (7) are equal to those in Eq. (6). Equation (7), which is a property of the bulk phase,

specifies a linear relation among μ_{As}, μ_{Ga}, and $\Delta\mu_{cat}$ that can be imposed on the surface by solving Eq. (7) for μ_{Ga} and substituting into Eq. (6) to find

$$\gamma = \left[E_f^{(slab)} - N_{cat}^{(slab)} E_f^{(In_yGa_{1-y}As)} - \mu_{As}\left(\widetilde{N}_{As}^{(slab)} - N_{cat}^{(slab)}\right) - \Delta\mu_{cat}\left(N_{In}^{(slab)} - yN_{cat}^{(slab)}\right)\right] / \left(A_{(1\times1)}N_{(1\times1)}\right). \tag{8}$$

It is common to define surface excess quantities, which in this case are the surface excess formation energy

$$E_f^{(xs)} = \left(E_f^{(slab)} - N_{cat}^{(slab)} E_f^{(In_yGa_{1-y}As)}\right) / \left(A_{(1\times1)}N_{(1\times1)}\right), \tag{9}$$

the surface excess As composition,

$$x_{As}^{(xs)} = \left(\widetilde{N}_{As}^{(slab)} - N_{cat}^{(slab)}\right) / \left(A_{(1\times1)}N_{(1\times1)}\right), \tag{10}$$

and the surface excess In composition,

$$x_{In}^{(xs)} = \left(N_{In} - yN_{cat}^{(slab)}\right) / \left(A_{(1\times1)}N_{(1\times1)}\right). \tag{11}$$

However, because we find with DFT that In is completely insoluble in GaAs as $T \to 0$, we will assume that y is zero when calculating γ. In terms of these definitions, the surface free energy becomes

$$\gamma = E_f^{(xs)} - \mu_{As}x_{As}^{(xs)} - \Delta\mu_{cat}x_{In}^{(xs)}. \tag{12}$$

Because the formation energy is measured relative to fixed-energy bulk reference states of bulk As, InAs, and GaAs, the chemical potential domain over which the reconstruction-terminated GaAs is stable relative to nucleation of other bulk phases is easily specified. When $y = 0$, as we assume here, the surface becomes unstable relative to bulk As condensation at $\mu_{As} > 0$ and becomes unstable relative to bulk InAs at $\Delta\mu_{cat} > 0$. Additionally, the surface becomes unstable relative to bulk Ga condensation at $\mu_{As} < \mathcal{E}_0^{(GaAs)} - \mathcal{E}_0^{(Ga)} - \mathcal{E}_0^{(As)} \approx -0.7$ eV. Due to the surfactant nature of InAs on GaAs, bulk GaAs is stable relative to both bulk InAs and bulk In over a very wide range of chemical potentials, according to DFT. This is the range of chemical potentials that permit a physically realizable InAs/GaAs wetting layer at equilibrium, and it is the range we have considered in constructing our phase diagram.

We performed a gound-state reconstruction search by fitting a cluster expansion Hamiltonian for each reconstruction prototype, resulting in separate Hamiltonians for the (2×4), (4×3), and $c(4 \times 4)$, each of which was used to screen for ground-state configurations of its respective prototype. The calculation-screening procedure was continued until self-consistency, meaning that all predicted ground-state configurations of the final cluster expansions are contained in the database of DFT-calculated configurations. This database was then used to construct the complete wetting layer phase diagram by finding the reconstruction that minimizes the 0-K surface free energy at each combination of chemical potentials μ_{As} and $\Delta\mu_{cat}$.

The collection of chemical potential pairs $(\mu_{As}, \Delta\mu_{cat})$ at which surface energies of two minimal-energy ground states cross specify a reconstruction phase boundary. Given the definitions of the chemical potentials, a Clausius-Clapeyron relation can be obtained that relates the slope of a phase boundary to the change in composition across the boundary. This is stated as

$$\frac{d\Delta\mu_{cat}}{d\mu_{As}} = -\frac{\Delta x_{As}^{(xs)}}{\Delta x_{In}^{(xs)}}, \tag{13}$$

which can be interpreted by considering its limiting cases. A phase boundary perpendicular to the $\Delta\mu_{cat}$ axis (i.e., having zero slope) separates two phases having the same $x_{As}^{(xs)}$, and thus only the surface In composition $x_{In}^{(xs)}$ changes as the boundary is crossed at 0 K. A phase boundary perpendicular to the μ_{As} axis (i.e., having infinite slope) separates two phases having the same $x_{In}^{(xs)}$. This relation can significantly simplify the graphical interpretation of a multicomponent surface phase diagram depicted in terms of chemical potentials.

III. RESULTS AND DISCUSSION

To construct the phase diagram, we calculated a total of 840 surface energies with DFT, corresponding to various alloy configurations of Ga, In, and As atoms over the substitutional sites of each of the surface reconstruction prototypes as specified in Fig. 1. These calculations included 378 configurations of the (2×4) 296 configurations of the (4×3), and 166 configurations of the $c(4 \times 4)$. However, using the cluster expansion as a tool for performing the ground-state search allowed us to screen a much larger set of candidate configurations [4]. In fact, with the cluster expansion to guide our search, we are limited mainly by our ability to enumerate candidate configurations and to manage the very large data sets that are generated. Using the cluster expansion for each prototype, we screened over 30 000 configurations of the (4×3) prototype and 200 000 configurations of the $c(4 \times 4)$ prototype. Monte Carlo simulated annealing, which also uses the cluster expansion to screen many thousands of configurations, was used to sample (4×4) and (2×8) configurations of the (2×4) prototypes. As new ground states were identified, their energies were calculated with DFT and incorporated into the cluster expansion training sets until no new ground states were identified. Given the number of configurations that we have been able to consider, we can be relatively certain to have identified the most important configurational ground states of the prototypes under consideration.

The predicted surface phase diagram of the InAs/GaAs(001) wetting layer, obtained by identifying the configuration that minimizes Eq. (12) at each chemical-potential pair, is shown in Fig. 2(a). Solid boundaries on the phase diagram indicate transitions between distinct structural prototypes, while dashed boundaries indicate transitions between different configurations of the structural prototype. Illustrations of all configurational groundstates can be found in Ref. [39]. According to Fig. 2(a), which was determined directly from DFT energy data, each prototype depicted in Fig. 1 has stable configurations within at least a small region of chemical potential. Notably, both the (4×3) and $\alpha2(2 \times 4)$ are predicted to be alloy-stabilized, in that they are not predicted to be stable on the pure GaAs(001) surface at the low extremes of $\Delta\mu_{cat}$ but become stable as In is added to the surface. Interestingly, the (4×3) is predicted stable only within a small "island" of chemical potential within the
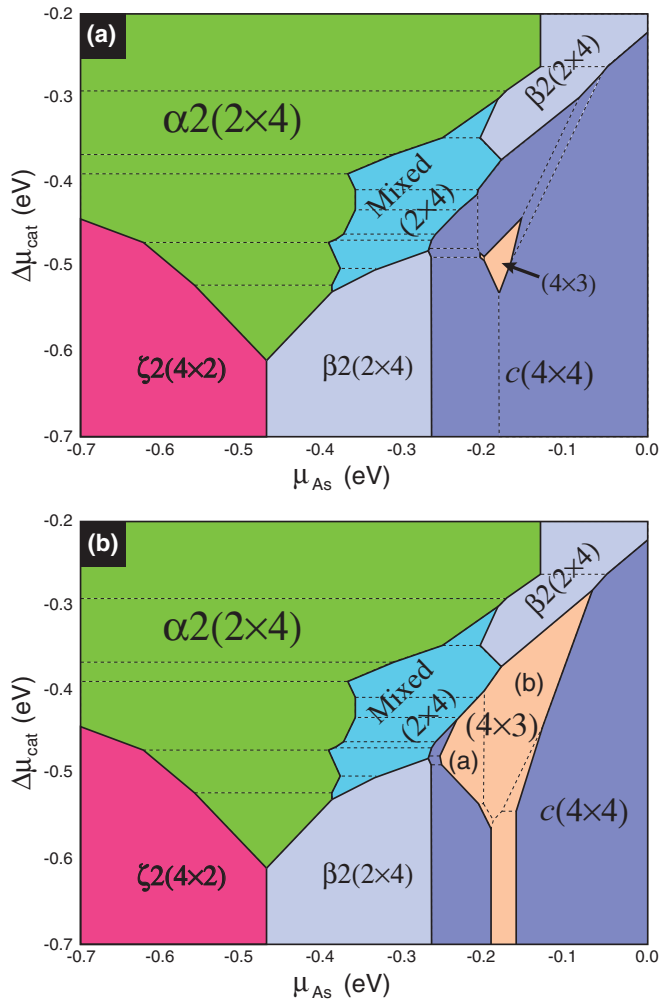
FIG. 2. (Color online) Surface phase diagrams of the InAs wetting layer on GaAs(001), constructed by finding the set of surface reconstructions that minimize the 0 K DFT surface energy at each chemical potential point. Surface In composition increases along the vertical axis, and surface As composition increases along the horizontal axis. Two cases are shown: (a) the phase diagram obtained directly from DFT calculations and (b) the phase diagram obtained by considering an 8-meV/$A_{(1\times1)}$ negative shift to the (4 × 3) surface energies. In both cases, solid lines indicate transitions between distinct structural prototypes, while dashed lines indicate transitions between different configurations of the structural prototype. Illustrations of all configurational ground states can be found in Ref. [39].

consist of patchwork-tiled (2 × 4) cells of both $\alpha2(2 \times 4)$ and $\beta2(2 \times 4)$ are stable over a relatively large region. The high density of configuration phase boundaries in the region where the mixed (2 × 4) occurs is consistent with previous results demonstrating the tendency of the mixed (2 × 4) surface phase on InAs/GaAs(001) to disorder at finite temperature [15]. The robust stability of $\alpha2(2 \times 4)$ over a large section of the As-poor, In-rich region of the phase diagram in Fig. 2 moreover suggests that the results presented in Ref. [15] likely have broad relevance to the finite-temperature thermodynamics of the InAs/GaAs(001) wetting layer.

The most intriguing features of the surface phase diagram in Fig. 2(a) are the existence and topology of the region of (4 × 3) phase stability. Within the experimental literature on the In$_x$Ga$_{1-x}$As (001) surface and the InAs/GaAs (001) wetting layer, the reconstructions with ($n \times 3$) periodicity are largely regarded as being In-induced surface reconstructions that are not present on the pure GaAs (001) surface [40–42]. However, it is evident from the broader experimental literature on GaAs(001) [17,18,21] and from previous theoretical results [5] that such a surface should exist at compositions intermediate to $c(4 \times 4)$ and $\beta2(2 \times 4)$ even before In deposition. This discrepancy is likely due to the weak thermodynamic driving force to nucleate (4 × 3) domains when the metastable $c(4 \times 4)$ reconstruction is present on the surface. However, it is known that alloying greatly enhances stability of the (4 × 3) reconstruction phase [12,13,22], and the predicted free energies seems to follow this trend, since the DFT surface free energies of (4 × 3) configurations, which are nearly stable at low $\Delta\mu_{cat}$ become stable when $\Delta\mu_{cat}$ is increased. Nevertheless, the small region of (4 × 3) stability in Fig. 2(a) is in contradiction to the robustness with which the (4 × 3) surface is observed experimentally on the InAs/GaAs(001) wetting layer.

In order to better understand the discrepancy between experimental observations of the (4 × 3) surface phase and the phase diagram in Fig. 2(a), we have conducted a sensitivity analysis to determine the robustness of the phase diagram topology with respect to small errors in the calculated energies due to DFT approximations and numerical convergence. In a previous first-principles analysis of the finite temperature GaAs(001) surface, we estimated a lower bound on the error of DFT-calculated surface energies and used rigorous finite-temperature simulations to construct a GaAs(001) phase diagram and calibrate our DFT errors to the experimental phase diagram [5]. Given the results of that calibration, it is reasonable to assume that DFT may predict a surface free energy for the alloyed (4 × 3) that is slightly too high relative to its surrounding phases; moreover, the (4 × 3) has a slightly higher vibrational entropy (and, consequently, lower free energy) than its surrounding phases, which acts to enhance its stability at finite temperature. In order to explore the effect of these and other phenomena that might cause relative shifts in the surface energies of the reconstruction prototypes considered here, we have constructed a second surface phase diagram for the InAs/GaAs wetting layer, shown in Fig. 2(b), that assumes that DFT predicts surface energies for the (4 × 3) prototype that are slightly too high. The resulting sensitivity-inferred phase diagram shown in Fig. 2(b) was constructed by subtracting a constant shift of 8.0 meV/$A_{(1\times1)}$ from the DFT

larger region of $c(4 \times 4)$ stability. This behavior suggests that, similarly to the unalloyed case, the (4 × 3) and $c(4 \times 4)$ are very close in surface free energy, and their surface formation energies have very similar dependence on stoichiometry.

The phase diagram in Fig. 2(a) additionally contextualizes previously reported first-principles analysis of the (2 × 4) phase [15] by revealing the relation of the (2 × 4) to the other reconstruction prototypes that are stable on the InAs/GaAs(001) wetting layer. In particular, the comprehensive wetting-layer phase diagram in Fig. 2(a) shows that a large range of In-containing $\beta2(2 \times 4)$ configurations are inaccessible, or at least metastable with respect to the $c(4 \times 4)$. By comparison, the hybrid (2 × 4) configurations, which

surface energies of all (4×3) configurations; this is slightly smaller than the 8.5-meV/$A_{(1 \times 1)}$ error calibration determined in Ref. [5].

Applying this small 8-meV/$A_{(1 \times 1)}$ shift to the (4×3) surface energies results in a significant change in the phase diagram topology. In Fig. 2(b), the (4×3) reconstruction phase is now stable at the unalloyed boundary of the phase diagram, matching the result obtained in Ref. [5]. Additionally, the alloy-induced stabilization of the (4×3) is markedly enhanced. Whereas the original phase diagram exhibited only a small island of (4×3) stability, the sensitivity-inferred phase diagram shows that a large region of $c(4 \times 4)$ stability becomes displaced by the (4×3). The two predominant $c(4 \times 4)$ configurations that remain in the inferred phase diagram correspond to the $c(4 \times 4)$-γ and $c(4 \times 4)$-α, which have been discussed in detail elsewhere [5,43]. Additionally, the region of (4×3) stability in the inferred phase diagram shares a phase boundary with the (2×4) reconstruction phase. This is a particularly notable result, as the experimentally-measured surface phase diagram of the InAs wetting layer on GaAs(001) implies that such a phase boundary should exist [12]. The same experimental phase diagram also indicates that the (4×3) surface phase should share a boundary with the $c(4 \times 4)$ surface phase, and a number of STM measurements show that the two phases can coexist on the wetting layer [10,13].

Although neither of the phase diagrams in Fig. 2 yield direct predictions about finite-temperature behavior of the InAs/GaAs(001) wetting layer, they do provide insights that enable us to better interpret existing experimental findings as well as identify consideration essential to formulating rigorous models for finite-temperature simulation of the wetting layer. As we have shown previously for the (2×4) reconstruction phase [15], the existence of many different ground-state configurations of a reconstruction prototype within a narrow region of chemical potential suggests a tendency for that prototype to disorder at low temperatures. Although a finite-temperature analysis has demonstrated an entropic stability enhancement of the $c(4 \times 4)$ relative to the (4×3) at high temperatures on the pure GaAs(001) surface [5], the phase diagram in Fig. 2(b) shows that there are relatively more alloyed ground states of the (4×3) prototype than the $c(4 \times 4)$ prototype once In is present on the surface. We thus anticipate that configurational entropy may have a further stabilizing effect on the (4×3) prototype on the InAs/GaAs(001) wetting layer.

In a strict sense, the finite-temperature stability of a reconstruction prototype depends on the density of structural, configurational, and vibrational states that are close in energy to the 0-K ground states. Although structural and configurational effects typically overwhelm vibrational effects, in situations where structural and configurational energies are very similar, as they are for the $c(4 \times 4)$ and (4×3) prototypes, vibrational effects become essential to predicting phase stability. Moreover, the structural similarities of the $c(4 \times 4)$ and (4×3) prototypes (e.g., they both primarily consist of dimer rows along the [1$\bar{1}$0] direction), along with their proximity in energy, suggest that *structural disorder* may play an important role in the finite-temperature thermodynamics of the InAs/GaAs(001) wetting layer. In this scenario, the system samples a nontrivial portion of microstates that share attributes of both the $c(4 \times 4)$ and (4×3) but cannot be classified as
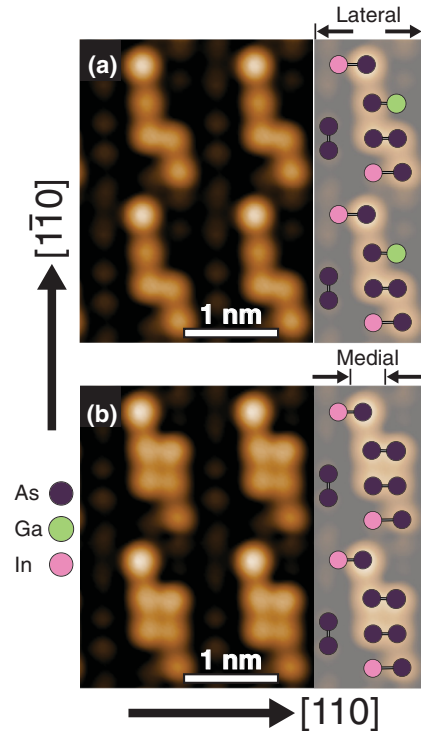

FIG. 3. (Color online) Simulated scanning tunneling micrographs of predicted (4×3) ground-state reconstructions of the InAs/GaAs(001) wetting layer. The reconstructions are configurations of the (4×3) reconstruction prototype illustrated in Fig. 1. Labels (a) and (b) correspond to labeled phases in Fig. 2(b). Configuration (a) has two In and one Ga per unit cell, relative to the all-As $h0(4 \times 3)$ configuration; configuration (b) has two In per unit cell. Simulated micrographs correspond approximately to imaging conditions at a 1-V forward bias. Medial and lateral designations are used in the text to refer to specific dimerized sites of the (4×3) prototype.

one or the other. This is especially likely given the observation of both structural disorder [12,40] and reconstruction coexistence [10,13] in STM of the (4×3) and $c(4 \times 4)$ on InAs/GaAs (001). Rigorous treatment of these considerations in a finite-temperature simulation would necessitate the development of a complex lattice model that describes both reconstruction prototypes on an equal footing and incorporates long-range strain interactions, which become important when there is structural inhomogeneity of the surface [44].

The (4×3) configuration that occurs in the unalloyed region at the bottom of the phase diagram in Fig. 2(b) is the $\beta(4 \times 3)$ reconstruction [39], which is a well-known surface reconstruction of GaSb(001) [30] in which all dimers are As–As homodimers except for a Ga atom that substitutes at the lateral position of the [110]-oriented dimer that is shifted relative to the prominent three-dimer block (with respect to the illustration in Fig. 1). The reconstructions that comprise the two predominant alloyed configurations [labeled (a) and (b) in Fig. 2] of the energy-shifted (4×3) have As-cation ordering that is quite distinct from that of the $\beta(4 \times 3)$ reconstruction. These two configurations are illustrated in the insets of Figs. 3(a) and 3(b). In contrast to the $\alpha(4 \times 3)$

and $\beta(4 \times 3)$ configurations, which are energetically preferred on pure GaAs and GaSb, the alloyed (4×3) configurations exhibit a "staircase" or "chair" ordering motif, with one In atom substituting at the lateral site of the shifted dimer and another In atom substituting in a medial site of the nearby three-dimer block (the distinction between medial and lateral sites is indicated in Fig. 3). This ordering motif is somewhat unexpected, given the high energy of Ga substitution at medial dimer sites of the (4×3) prototype on unalloyed GaAs(001) [5].

The unique alloy ordering of the most stable configurations of the alloyed (4×3) prototype should appear quite different under STM than either the $\alpha(4 \times 3)$ or $\beta(4 \times 3)$ [30]. To demonstrate this, we have simulated filled-state STM micrographs for the two alloyed (4×3) configurations, which are shown in Figs. 3(a) and 3(b). The STM simulation uses the real-space partial charge of the relaxed surface corresponding to electronic states within a specified range of the Fermi level, calculated using DFT. The micrographs are obtained by finding an isocharge surface of the partial charge as the surface is approached from vacuum. This simulation scheme measures the predicted real-space distribution of states near the valence-band maximum, which, in the context of the established theory for STM [45], roughly approximates STM tunneling current at a voltage bias proportional to the specified energy range. Partial charge densities were obtained using the implementation for bandwise charge decomposition included with VASP [33].

The simulated micrographs obtained for the stable configurations of the alloyed (4×3) differ significantly from simulated micrographs of either the $\alpha(4 \times 3)$ or $\beta(4 \times 3)$ [30]. In particular, the "chair" motif of the alloyed (4×3) configurations is easily discerned, and the As atom of the shifted In-As heterodimer is visibly brighter than the other atoms. Although anion species are typically brighter in STM due to their valence-band dangling orbitals, As atoms on the shifted heterodimers in Figs. 3(a) and 3(b) are brighter than even the surrounding As atoms in the same monolayer. The reason for the enhanced contrast of this As site remains unclear, as the relaxed position of the bright As site is not at a higher elevation than that of the surrounding anions. However, the bonds of the shifted-dimer As site form relatively narrow bond angles, ranging from $90.3°$–$100.7°$, compared to $94.8°$–$104.3°$ for the same site of the unalloyed $\beta(4 \times 3)$. The narrower bonding angles may force the site's filled sp^3-type dangling orbital to project more nearly perpendicular to the surface, enhancing its apparent brightness under STM.

The As-cation ordering motif, together with the enhanced contrast of the alloyed (4×3) in simulated STM has important relevance to experimental results. Although published micrographs of the $(n \times 3)$ reconstruction on the InAs/GaAs(001) wetting layer are typically much more disordered than the simulated micrographs in Figs. 3(a) and 3(b), they do share common traits. In particular, many published micrographs of the $(n \times 3)$ surface phase on the InAs/GaAs(001) wetting layer have the appearance of narrow, meandering rows along $[1\bar{1}0]$, with brighter features occurring at a periodicity of ~ 4 times the surface lattice parameter [10,12,13,40]. At short length scales, many of these experimental micrographs of the $(n \times 3)$ bear a striking resemblance to the simulated micrograph in Fig. 3(a), suggesting either that it is a fundamental unit of the $(n \times 3)$ surface, or that it shares a fundamental motif with the $(n \times 3)$ such as the shifted heterodimer and adjacent heterodimers in Fig. 3(a).

IV. SUMMARY

We have constructed a comprehensive 0-K phase diagram for the complex InAs/GaAs(001) wetting layer from first principles. We combined large-scale DFT calculations with the cluster expansion formalism to identify the ground-state reconstructions of the surface. These tools were used together to construct a very large database of first-principles surface energies for low-energy configurations of In, As, and Ga atoms at the undercoordinated sites of three different reconstruction prototypes, which was further leveraged using the cluster expansion formalism to screen thousands of additional configurations. The resulting phase diagram represents a particularly comprehensive prediction for the equilibrium structure of the InAs/GaAs(001) surface alloy, and the large number and variety of configurations that are predicted to be stable illustrate the necessity of conducting such far-reaching ground state searches.

The predicted phase diagram corroborates a number of trends that have been observed experimentally, including the alloy-induced stability of the (4×3) and $\alpha2(2 \times 4)$ surface phases. However, better agreement with experiment can be obtained by applying an 8.0-meV/$A_{(1 \times 1)}$ negative shift to the (4×3) surface energy, consistent with experimentally calibrated DFT error estimates for GaAs(001) [5]. With the shift applied, the phase diagram exhibits close agreement with many of the experimental trends of the InAs/GaAs wetting layer behavior. These include the existence of an unalloyed (4×3), the shared boundary between (4×3) and (2×4) surface phases, and the significant alloy-induced enhancement in (4×3) stability. Moreover, simulated STM micrographs of stable configurations of the alloyed (4×3) differ significantly from the simulated or measured STM of the low-energy configurations on un-alloyed surfaces. The alloyed (4×3) configurations that are predicted to be stable instead exhibit a characteristic bright-spot–chair motif that at short length scales bears a strong resemblance to experimental STM of the InAs/GaAs(001) wetting layer.

[1] R. Osório, J. E. Bernard, S. Froyen, and A. Zunger, Phys. Rev. B **45**, 11173 (1992).

[2] S. Froyen and A. Zunger, Phys. Rev. B **53**, 4570 (1996).

[3] Z. Kollonitsch, H.-J. Schimper, U. Seidel, K. Mller, S. Neumann, F.-J. Tegude, F. Willig, and T. Hannappel, J. Cryst. Growth **287**, 536 (2006).

[4] J. C. Thomas, N. A. Modine, J. M. Millunchick, and A. Van der Ven, Phys. Rev. B **82**, 165434 (2010).

[5] J. C. Thomas, A. Van der Ven, J. M. Millunchick, and N. A. Modine, Phys. Rev. B **87**, 075320 (2013).

[6] A. Duzik, J. C. Thomas, A. van der Ven, and J. M. Millunchick, Phys. Rev. B **87**, 035313 (2013).

[7] J. M. Sanchez, F. Ducastelle, and D. Gratias, Physica A **128**, 334 (1984).

[8] J. Belk, J. Sudijono, D. Holmes, C. McConville, T. Jones, and B. Joyce, Surf. Sci. **365**, 735 (1996).

[9] S. Franchi, A. Bosacchi, F. Colonna, P. Pascarella, P. Allegri, and V. Avanzini, J. Cryst. Growth **150**, 185 (1995).

[10] M. Xu, Y. Temko, T. Suzuki, and K. Jacobi, Surf. Sci. **580**, 30 (2005).

[11] M. Kroutvar, Y. Ducommun, D. Heiss, M. Bichler, D. Schuh, G. Abstreiter, and J. Finley, Nature **432**, 81 (2004).

[12] J. Belk, C. McConville, J. Sudijono, T. Jones, and B. Joyce, Surf. Sci. **387**, 213 (1997).

[13] C. Prohl, B. Höpfner, J. Grabowski, M. Dähne, and H. Eisele, J. Vac. Sci. Technol. B **28**, C5E13 (2010).

[14] A. Urbańczyk and R. Nötzel, J. Cryst. Growth **341**, 24 (2012).

[15] J. C. Thomas, J. M. Millunchick, N. A. Modine, and A. Van der Ven, Phys. Rev. B **80**, 125315 (2009).

[16] A. Van der Ven, J. Thomas, Q. Xu, and J. Bhattacharya, Math. Comput. Simul. **80**, 1393 (2010).

[17] L. Däweritz and R. Hey, Surf. Sci. **236**, 15 (1990).

[18] I. Chizhov, G. Lee, R. F. Willis, D. Lubyshev, and D. L. Miller, Phys. Rev. B **56**, 1013 (1997).

[19] W. Schmidt, Appl. Phys. A-Mater. **75**, 89 (2002).

[20] A. Ohtake, Surf. Sci. Rep. **63**, 295 (2008).

[21] M. Masnadi-Shirazi, D. Beaton, R. Lewis, X. Lu, and T. Tiedje, J. Cryst. Growth **338**, 80 (2012).

[22] Jan Grabowski and Christopher Prohl and Britta Höpfner and Mario Dähne and Holger Eisele, Appl. Phys. Lett. **95**, 233118 (2009).

[23] A. Duzik, J. C. Thomas, J. M. Millunchick, J. Lng, M. Punkkinen, and P. Laukkanen, Surf. Sci. **606**, 1203 (2012).

[24] A. Chakrabarti, P. Kratzer, and M. Scheffler, Phys. Rev. B **74**, 245328 (2006).

[25] E. Penev and P. Kratzer, in *Quantum Dots: Fundamentals, Applications, and Frontiers*, edited by B. A. Joyce, P. C. Kelires, A. G. Naumovets, and D. D. Vvedensky, NATO Science Series II-Mathematics Physics and Chemistry Vol. 190 (NATO, Sci Affairs Div; British Assoc Crystal Growth, Crete, Greece, 2005), pp. 27–42.

[26] J. E. Bickel, N. A. Modine, A. Van der Ven, and J. M. Millunchick, Appl. Phys. Lett. **92**, 062104 (2008).

[27] S.-H. Lee, W. Moritz, and M. Scheffler, Phys. Rev. Lett. **85**, 3890 (2000).

[28] J.-H. Cho, S. B. Zhang, and A. Zunger, Phys. Rev. Lett. **84**, 3654 (2000).

[29] M.D. Pashley, Phys. Rev. B **40**, 10481 (1989).

[30] W. Barvosa-Carter, A. S. Bracker, J. C. Culbertson, B. Z. Nosho, B. V. Shanabrook, L. J. Whitman, H. Kim, N. A. Modine, and E. Kaxiras, Phys. Rev. Lett. **84**, 4649 (2000).

[31] D. L. Feldwinn, J. B. Clemens, J. Shen, S. R. Bishop, T. J. Grassman, A. C. Kummel, R. Droopad, and M. Passlack, Surf. Sci. **603**, 3321 (2009).

[32] J. J. K. Lång, M. P. J. Punkkinen, P. Laukkanen, M. Kuzmin, V. Tuominen, M. Pessa, M. Guina, I. J. Väyrynen, K. Kokko, B. Johansson, and L. Vitos, Phys. Rev. B **81**, 245305 (2010).

[33] G. Kresse and J. Furthmüller, Phys. Rev. B **54**, 11169 (1996).

[34] D. M. Ceperley and B. J. Alder, Phys. Rev. Lett. **45**, 566 (1980).

[35] J. P. Perdew and A. Zunger, Phys. Rev. B **23**, 5048 (1981).

[36] D. Vanderbilt, Phys. Rev. B **41**, 7892 (1990).

[37] Y.-M. Juan and E. Kaxiras, Phys. Rev. B **48**, 14944 (1993).

[38] It is perfectly valid to choose other reference states (e.g., bulk Ga, bulk In, and molecular As$_4$), but our particular choices simplify the mathematical expression for γ, as we define it, and make chemical potential values more physically meaningful.

[39] See Supplemental Material at http://link.aps.org/supplemental/10.1103/PhysRevB.89.205306 for illustrations of all reconstructions corresponding to the phase diagrams in Figs. 2(a) and 2(b).

[40] T. J. Krzyzewski, P. B. Joyce, G. R. Bell, and T. S. Jones, Surf. Sci. **517**, 8 (2002).

[41] C. Pearson, C. Dorin, J. M. Millunchick, and B. G. Orr, Phys. Rev. Lett. **92**, 056101 (2004).

[42] P. Bone, J. Ripalda, G. Bell, and T. Jones, Surf. Sci. **600**, 973 (2006).

[43] E. Penev, P. Kratzer, and M. Scheffler, Phys. Rev. Lett. **93**, 146102 (2004).

[44] J. B. Hannon, F.-J. Meyer zu Heringdorf, J. Tersoff, and R. M. Tromp, Phys. Rev. Lett. **86**, 4871 (2001).

[45] J. Tersoff and D. R. Hamann, Phys. Rev. B **31**, 805 (1985).